Title
Inducible Expression of CXCL1 within the Central Nervous System Amplifies Viral-Induced Demyelination

Journal
The Journal of Immunology, 196(4)

ISSN
0022-1767

Authors
Marro, Brett S
Grist, Jonathan J
Lane, Thomas E

Publication Date
2016-02-15

DOI
10.4049/jimmunol.1501802

Peer reviewed

Inducible Expression of CXCL1 within the Central Nervous System Amplifies Viral-Induced Demyelination

Brett S. Marro,* Jonathan J. Grist,† and Thomas E. Lane†

The functional role of the ELR$^+$ chemokine CXCL1 in host defense and disease following infection of the CNS with the neurotropic JHM strain of mouse hepatitis virus (JHMV) was examined. Mice in which expression of CXCL1 is under the control of a tetracycline-inducible promoter active within glial fibrillary acidic protein–positive cells were generated and this allowed for selectively increasing CNS expression of CXCL1 in response to JHMV infection and evaluating the effects on neuroinflammation, control of viral replication, and demyelination. Inducible expression of CNS-derived CXCL1 resulted in increased levels of CXCL1 protein within the serum, brain, and spinal cord that correlated with increased frequency of Ly6G$^+$CD11b$^+$ neutrophils present within the CNS. Elevated levels of CXCL1 did not influence the generation of virus-specific T cells, and there was no difference in control of JHMV replication compared with control mice, indicating that T cell infiltration into the CNS is CXCL1-independent. Sustained CXCL1 expression within the CNS resulted in increased mortality that correlated with elevated neutrophil infiltration, diminished numbers of mature oligodendrocytes, and an increase in the severity of demyelination. Neutrophil ablation in CXCL1-transgenic mice reduced the severity of demyelination in mice, arguing for a role for these cells in white matter damage. Collectively, these findings illustrate that sustained CXCL1 expression amplifies the severity of white matter damage and that neutrophils can contribute to this process in a model of viral-induced neurologic disease. ***The Journal of Immunology*****, 2016, 196: 1855–1864.**

Inoculation of susceptible mice with the neurotropic JHM strain of mouse hepatitis virus (JHMV) into the CNS results in widespread dissemination of virus, leading to infection and replication within glial cells. This is followed by infiltration of virus-specific T lymphocytes that control viral replication through cytokine secretion and cytolytic activity (1). Sterilizing immunity is not achieved, as viral Ag and viral RNA are detected within white matter tracts of surviving mice, resulting in demyelination that is amplified by inflammatory T cells and macrophages. In response to infection, numerous cytokines/chemokines are secreted by inflammatory leukocytes and resident cells of the CNS, generating an inflammatory milieu that contributes to host defense while also promoting disease. Our previous work has evaluated the functional roles for chemokines and chemokine receptors in orchestrating leukocyte recruitment into the CNS in response to JHMV infection that aid in host defense as well as their contribution to demyelination (2–5).

Among the chemokines expressed during acute and chronic JHMV-induced neurologic disease are the ELR$^+$ CXC chemokines CXCL1, CXCL2, and CXCL5 and its signaling receptor CXCR2 (4, 6). Following JHMV infection of the CNS, expression of CNS-derived ELR$^+$ ligands promote the migration of CXCR2-expressing neutrophils (Ly6G/C^{hi}CD11b$^+$) to the blood–brain barrier (BBB), where they can assist in breaking down structural components of the glial limitans through release of matrix metalloproteinases (MMPs) from preformed granules. Indeed, Ab-mediated neutralization of CXCR2 within JHMV-infected mice prevented neutrophil migration to the CNS, and this was associated with a significant increase in mortality and inefficient control of virus replication as a result of impaired parenchymal access of virus-specific T cells (4). Anti-CXCR2 treatment was also found to diminish macrophage recruitment to the CNS as well, making it challenging to define the precise contributions of both immune cell subsets in establishing host defense while also promoting disease when CXCR2 signaling is neutralized (4). Other studies have demonstrated that neutrophil depletion in JHMV-infected mice in which monocyte trafficking to the CNS is compromised does not alter early CNS inflammation, clinical disease severity, or death, but rather it limits parenchymal access of leukocytes at later times following infection, suggesting that neutrophils and monocytes may act separately to shape adaptive immunity following JHMV infection of the CNS (7, 8).

The present study was undertaken to expand our understanding of how ELR$^+$ chemokines influence host defense and disease progression following JHMV infection of the CNS. To this end, we have generated mice in which expression of CXCL1 is under the control of a tetracycline-inducible promoter that is active within glial fibrillary acidic protein (GFAP)$^+$ cells that express an enhanced version of the reverse tetracycline transactivator (rtTA*M2) protein. The successful generation of these pBI-CXCL1-rtTA mice has allowed us to selectively increase CNS expression of CXCL1 in adult mice following JHMV-induced disease and evaluate the effects on neuroinflammation, control of viral replication, and demyelination.

*Department of Molecular Biology and Biochemistry, University of California, Irvine, Irvine CA 92697; and †Department of Pathology, University of Utah School of Medicine, Salt Lake City, UT 84112

ORCID: 0000-0001-5269-9202 (J.J.G.).

Received for publication August 10, 2015. Accepted for publication December 16, 2015.

This work was supported by National Institutes of Health Grant R01NS041249 (to T.E.L.). B.S.M. was supported by National Institutes of Health T32 Training Grant 5T32A1007319.

Address correspondence and reprint requests to Dr. Thomas E. Lane, Department of Pathology, University of Utah School of Medicine, Salt Lake City, UT 84112. E-mail address: tom.lane@path.utah.edu

The online version of this article contains supplemental material.

Abbreviations used in this article: BBB, blood–brain barrier; DOX, doxycycline; GFAP, glial fibrillary acidic protein; i.c., intracerebral(ly); JHMV, JHM strain of mouse hepatitis virus; MMP, matrix metalloproteinase; NaFl, sodium fluorescein; p.i., postinfection; rtTA, reverse tetracycline transactivator; tg, transgenic.

Materials and Methods

pBI-CXCL1 vector construction

CXCL1 cDNA incorporating XhoI and NheI restriction site ends was generated from the brains of C57BL/6 mice infected with 250 PFU JHMV. CXCL1 cDNA was cloned into a pBI-MCS-EGFP plasmid (9) downstream of a bidirectional tetracycline responsive element. The purified pBI-CXCL1 plasmid was linearized following an overnight incubation with AatII and AseI restriction enzymes to generate a 3350-bp fragment containing the pBI-CXCL1 construct.

Virus and mice

pBI-CXCL1 transgenic (tg) mice were generated by the University of California, Irvine tg mouse facility through DNA microinjection of fertilized C56BL/6 eggs using the linearized pBI-CXCL1 construct (9). The five resulting founder tg mice where mated to wild-type C57BL/6 mice to indentify F_1 offspring containing the transgene. To generate double-tg mice, hemizygous pBI-CXCL1 tgs were crossed to hemizygous GFAP-rtTA*M2 mice (The Jackson Laboratory), resulting in double-tg mice (pBI-CXCL1-rtTA), single-tg mice (rtTA-GFAP or pBI-CXCL1), or wild-type mice. For evaluation of CXCL1 induction in experimental mice, age-matched 5- to 6-wk-old single-tg or double-tg mice were infected intracerebrally (i.c.) with 250 PFU JHMV strain J2.2v-1 in 30 μl sterile HBSS; subsequently, animals were injected with doxycycline (Dox) (50 mg/kg via i.p. injection) starting at day 2 postinfection (p.i.) and continuing through day 12 p.i. SHAM-infected animals received 30 μl HBSS via i.c. injection. For viral titer analysis, one half of each brain or whole spinal cord was homogenized and used in a plaque assay as previously described (10).

Primary astrocyte cultures

Cortices from postnatal day 1 pBI-CXCL1-rtTA (double-tg) and rtTA-GFAP or pBI-CXCL1 (single-tg) mice were dissected and triturated according to previously published protocols (11). In brief, following removal of the meninges, cortical tissue was minced with a razor and placed in prewarmed DMEM containing papain to completely dissociate the tissue. Following further dissociation with a Pasteur pipette, single-cell suspensions were added to poly-D-lysine–coated culture flasks and grown for 9 d in DMEM supplemented with 10% FBS. Flasks were then transferred to an orbital shaker in a 5% CO_2 tissue culture incubator and shaken for ~16 h at 220 rpm to remove loosely adherent contaminating cells. Cells were passaged in 0.05% trypsin and replated. When cells regained confluency, 10 μM Ara-C (Sigma-Aldrich, St. Louis, MO) was added for 3 d to kill dividing cells. Cells were passaged again and added to 24-well culture dishes or Nunc Lab-Tek II chamber slides (Thermo Fisher Scientific, Waltham, MA).

Gene expression analysis

Total cDNA from brains and spinal cords of sham- and JHMV-infected mice at days 4, 7, and 12 p.i. was generated via SuperScript III (Life Technologies, Carlsbad, CA) following homogenization in TRIzol (Life Technologies). To determine relative CXCL1 mRNA expression, real-time SYBR Green analysis was performed using mouse β-actin primers (forward, 5′-GGCCCAGAGCAAGAGAGGTAT-3′; reverse, 5′-ACGCACGATTTCCCTCTCAGC-3′) and mouse CXCL1 primers (forward, 5′-GGCGCCTATCGCCAATG-3′; reverse, 5′-CTGGATGTTCTTGAGGTGAATCC-3′) using a Roche LightCycler 480 (12). CXCL1 expression was determined by normalizing the expression of each sample to β-actin and then quantifying fold change relative to sham-infected double-tg mice. Expression of defined mouse chemokine and cytokine genes within the CNS of experimental mice was determined using a mouse cytokine and chemokine RT^2 Profiler PCR array (Qiagen, Valencia, CA).

ELISA

Assessment of CXCL1 protein within the supernatants of Dox-treated astrocyte cultures was determined using a CXCL1 (KC) DuoSet sandwhich ELISA kit (R&D Systems, Minneapolis, MN) according to manufacturer specifications. To determine CXCL1 protein levels within the spinal cords of double- and single-tg mice, spinal cords were homogenized in RIPA buffer and clarified by high-speed centrifugation. Following quantification of total protein, samples were diluted in RIPA buffer to a standard protein concentration before performing the ELISA assay.

Flow cytometry

Flow cytometry was performed to immunophenotype inflammatory cells entering the CNS using established protocols (3, 13). In brief, single-cell suspensions were generated from tissue samples by grinding with frosted microscope slides. Immune cells were enriched by a two-step Percoll cushion (90 and 63%) and cells were collected at the interface of the two Percoll layers. Before staining with the fluorescent Abs, isolated cells were incubated with anti-CD16/32 Fc Block (BD Biosciences, San Jose, CA) at a 1:200 dilution. Immunophenotyping was performed using either rat anti-mouse IgG or Armenian hamster anti-mouse IgG Abs for the following cell surface markers: F4/80 (Serotec, Raleigh, NC), MHV S510-tetramer (National Institutes of Health), MHV M133-tetramer (National Institutes of Health), CD4, CD8, Ly6g, CD11b, IFN-γ (BD Biosciences), and Ly6c (eBioscience, San Diego, CA). The following flow cytometric gating strategies were employed for immunophenotyping inflammatory infiltrates in the brain: neutrophils ($CD45^{hi}CD11b^{+}Ly6G^{+}$), monocytes ($CD45^{hi}CD11b^{+}Ly6C^{+}Ly6G^{-}$), macrophages ($CD45^{hi}CD11b^{+}F4/80^{+}$), microglia ($CD45^{lo}$, $CD11b^{+}$, $F4/80^{lo}$), M133-specific $CD4^{+}$ T cells ($CD45^{hi}$, $CD4^{+}$, M133-tetramer^{+}), and S510-specific $CD8^{+}$ T cells ($CD45^{hi}$, $CD8^{+}$, S510-tetramer^{+}).

Sodium fluorescein BBB permeability assay

JHMV-infected double- or single-tg mice received 100 μl 10% sodium fluorescein (NaFl) in PBS via i.p. injection. After 30 min, mice were euthanized and perfused with 30 ml PBS to remove NaFl from the vasculature. Brains and spinal cords were dissected, weighed, and homogenized in PBS. Homogenates were clarified by centrifugation at 500 × *g* for 10 min at 4°C. A 1:1 ratio of supernatant was combined with 15% trichloroacetic acid and incubated for 24 h at 4°C. Samples were centrifuged and supernatants were neutralized with 5 N NaOH. Fluorescence intensity was assessed with a Synergy H1 (BioTek, Winooski, VT) set at a 485 nm excitation, and NaFl concentrations were determined through extrapolation from a standard curve generated from defined NaFl concentrations.

Clinical severity and histopathology

Clinical disease severity was assessed using a four-point scoring scale as previously described (3). Mice were euthanized according to Institutional Animal Care and Use Committee guidelines and perfused with 30 ml 4% paraformaldehyde. Spinal cords were removed, fixed overnight in 4% paraformaldehyde at 4°C, and separated into eight 1.5-mm sections. Each section was cryoprotected in 20% sucrose for 5 d before embedding in OCT; 8-μm-thick coronal sections were cut and stained with Luxol fast blue and H&E. The severity of demyelination for each mouse was determined using 6–12 spinal cord coronal sections per mouse using either a previously described four-point scoring scale (14) and calculated as average ± SEM or determining the percentage demyelination using ImageJ software (National Institutes of Health).

Immunofluorescence

Spinal cord sections were processed as above. For immunofluorescence, slides were first desiccated for at least 2 h and blocked with 5% normal donkey serum with or without 0.3% Triton X-100. Primary Abs were incubated overnight at 4°C, including goat anti-CXCL1 1:50 (R&D Systems), rabbit anti-GFAP 1:500 (Life Technologies), rat anti-Ly6B.2 1:100 (Serotec, Raleigh, NC), rabbit anti-Iba11:500 (Wako Chemicals, Richmond, VA), and rabbit anti–GST-π 1:1000 (MBL International, Woburn, MA).

Neutrophil depletion

Mice received either 250 μg anti-Ly6g clone 1A8 or isotype control (Bio X Cell, West Lebanon, NH) via i.p. injection every other day beginning between days 3 and 15 p.i. Targeted depletion of neutrophils was confirmed by flow staining of circulating neutrophils at defined times after treatment with Ly6g-specific Ab.

Statistical analysis

Flow cytometric data were analyzed with FlowJo (Tree Star), and statistical analyses were performed using Prism (GraphPad Software)

Results

Dox treatment of pBI-CXCL1-rtTA double-tg mice elevates CXCL1 mRNA and protein within the CNS

In response to CNS infection of C57BL/6 mice with JHMV, the ELR^{+} chemokine CXCL1 is expressed at early times after infection and serves to attract CXCR2-expressing neutrophils to the CNS that aid in host defense by contributing to the

permeabilization of the BBB (4). To better understand how CXCL1 signaling affects host defense and disease progression following viral infection of the CNS, tg mice were engineered to use the tetracycline-controlled transcriptional activation system in which the human GFAP promoter drove expression of a modified version of the rtTA protein (rtTA*M2). Astrocytes were chosen for targeted expression of CXCL1, as previous studies (15–17) have shown these cells to be the primary source of CXCL1 in models of neuroinflammation as well as following infection of astrocytes with JHMV (5, 6). In the presence of Dox, transcription initiates at a tetracycline operon and leads to production of rCXCL1 mRNA transcripts. Double-tg mice (pBI-CXCL1-rtTA) were generated and genotyped to confirm that they incorporated both constructs (Fig. 1A). Characterization of double-tg mice revealed Dox-dependent expression of CXCL1 from cultured astrocytes as determined by immunofluorescence staining and ELISA (Fig. 1B, 1C).

We tested whether treatment of tg mice with Dox resulted in overproduction of CXCL1 within the brain and spinal cord of the CNS of JHMV-infected mice. Double-tg or single-tg mice were infected i.c. with JHMV (250 PFU) and subsequently treated daily with Dox (50 mg/kg) via i.p. injection starting at day 2 p.i. and continuing through day 12 p.i. (Fig. 2A). Dox treatment resulted in increased mRNA transcripts specific for CXCL1 in the brains of infected double-tg mice at days 4, 7, and 12 p.i. compared with single-tg mice (Fig. 2B). Similarly, CXCL1 transcripts were elevated in the spinal cords at days 4, 7 ($p < 0.05$), and 12 ($p < 0.01$) p.i. when compared with single-tg mice (Fig. 2C). To confirm that that CXCL1 mRNA was derived from the transgene and not from germline-encoded CXCL1, we employed quantitative PCR primers that specifically anneal to an untranslated region region specific for endogenous CXCL1 mRNA and not tg CXCL1. As shown in Fig. 2D, there was only a marginal increase in endogenously produced CXCL1 mRNA transcripts when compared with transgene-encoded CXCL1. These results confirm that increased CXCL1 mRNA transcripts are derived from the CXCL1 transgene. CNS-derived CXCL1 in Dox-treated double-tg mice resulted in increased CXCL1 protein in both the spinal cord (Fig. 2E) and serum (Fig. 2F) compared with single-tg mice at day 7 p.i. Immunofluorescence staining confirmed increased CXCL1 protein present within the CNS and astrocytes as the primary cellular source in Dox-treated double-tg mice (Fig. 2G). Finally, overproduction of rCXCL1 within the CNS of JHMV-infected mice did not result in increased expression of other proinflammatory cytokines and chemokines within the spinal cord (Fig. 2H) or brain (data not shown). These data demonstrate that double-tg mice are responsive to Dox treatment, resulting in increased levels of CXCL1 derived within the CNS, and this corresponds to elevated levels of circulating CXCL1 within the serum. However, CXCL1 overproduction does not impact the expression of other proinflammatory factors involved in JHMV host defense and disease.

CXCL1 overexpression increases morbidity/mortality in double-tg mice

Dox-induced overexpression of CXCL1 within the CNS resulted in a statistically significant increase in clinical disease severity (Fig. 3A) and this correlated with an increase in mortality (Fig. 3B). This was not associated with impaired ability to control viral infection in Dox-treated double-tg mice, as there were comparable titers in the brains at days 4 and 7 p.i. whereas lower viral titers ($p < 0.05$) were found in spinal cords at days 4 and 7 p.i. (Fig. 3C, 3D). Both double-tg and single-tg animals reduced CNS viral titers to below detectable titers as measured by plaque assay within the brain by day 12 p.i. (Fig. 3C) whereas viral titers within the spinal cord at day 12 p.i. were near the limit of detection (Fig. 3D). Moreover, no differences were observed with viral RNA load between double-tg and single-tg mice at day 12 p.i. (data not shown). Treatment of JHMV-infected astrocytes with rCXCL1 did not decrease viral titers, ruling out that CXCL1 did

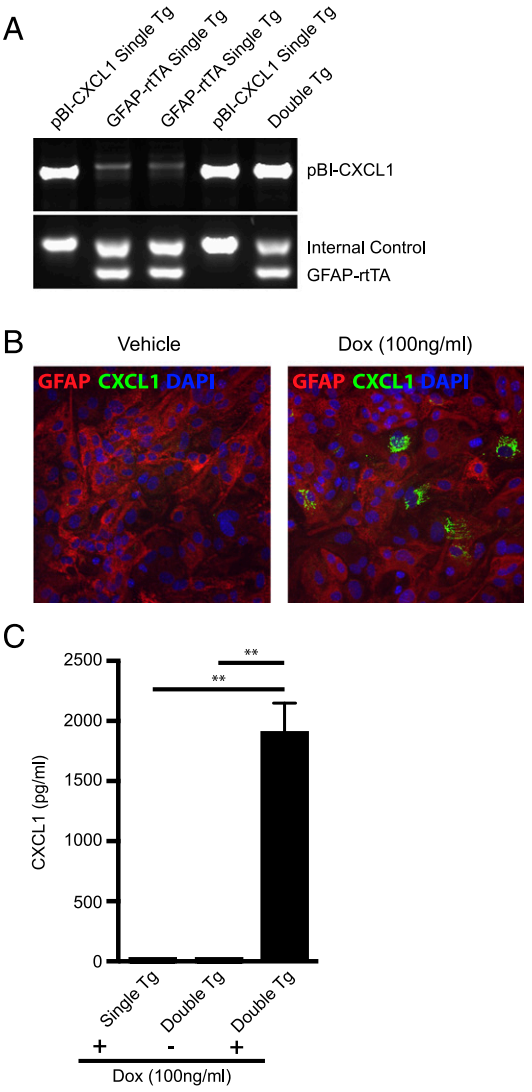

FIGURE 1. Generation and in vitro characterization of a Dox-inducible, astrocyte-specific CXCL1 overexpressing mouse line. (**A**) Double-tg mice utilizing the tetracycline operon–controlled Dox-inducible system were generated by crossing hemizygous human GFAP-rtTA*M2 mice to a tg mouse line incorporating a tetracycline responsive element driving expression of CXCL1 (pBI-CXCL1). Shown are PCR results with genomic DNA from mice revealing amplicons specific for either pBI-CXCL1 or GFAP-rtTa. The internal control was performed when detecting GFAP-rtTa amplicons according to defined Jackson Laboratory protocols. (**B**) Cortex tissue from double-tg and single-tg postnatal day 1 mice was dissociated and enriched for astrocytes. Following 24 h of Dox (100 ng/ml)-treated double-tg astrocyte cultures, immunofluorescence (original magnification ×20) confirmed CXCL1 expression within GFAP$^+$ astrocytes whereas vehicle treatment yielded no CXCL1 fluorescence. (**C**) Supernatants from Dox-treated double-tg and single-tg astrocytes cultures were collected and levels of CXCL1 were measured by ELISA. In the presence of Dox, double-tg cultures yielded significantly elevated CXCL1 protein levels, whereas single-tg cultures did not. Data from (C) represent supernatants pooled from triplicate wells derived from three separate double-tg and single-tg mouse cultures. Data are presented as average ± SEM; statistical significant was measured with an unpaired two-tailed Student *t* test. $^{**}p < 0.01$.

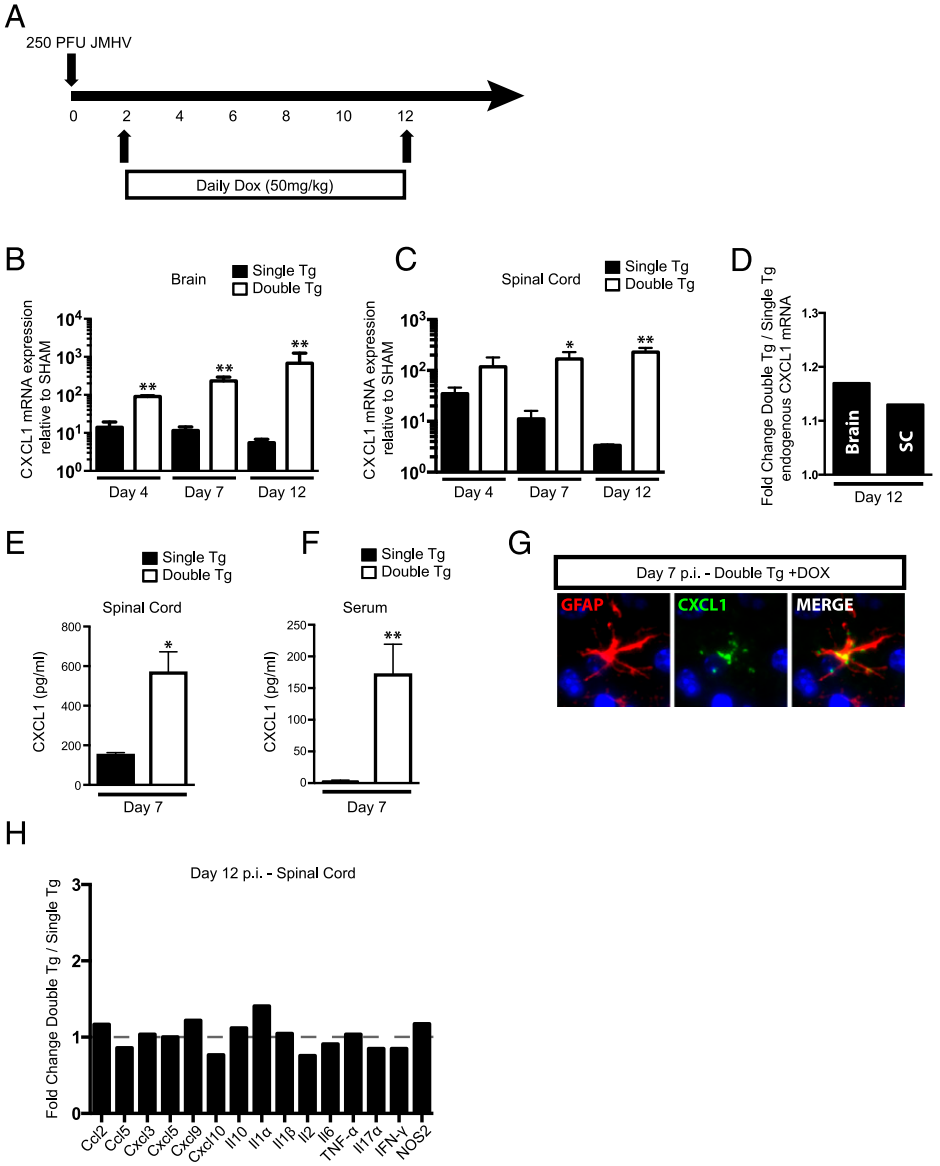

FIGURE 2. CXCL1 is induced in vivo following administration of Dox into double-tg mice during acute JHMV infection. (**A**) To test the ability of Dox to induce CXCL1 overproduction in vivo, double-tg and single-tg mice were infected with 250 PFU JHMV and treated daily with 50 mg/kg Dox between days 2 and 12 p.i. (**B**) Administration of Dox to double-tg mice resulted in a significant increase in the expression of CXCL1 mRNA compared with Dox-treated single-tg mice within the brain at days 4, 7, and 12 p.i. as measured by quantitative real-time PCR. (**C**) Within the spinal cord, dox-treated double-tg mice had statistically significant increases in CXCL1 mRNA expression over Dox-treated single-tg mice at days 7 and 12 p.i. (**D**) CXCL1 transgene expression within the brain and spinal cord did not impact endogenous CXCL1 production within Dox-treated double-tg mice compared with Dox-treated single-tg mice. Overproduction of CXCL1 protein was observed within the spinal cord at day 7 p.i. within double-tg mice (**E**), and this correlated with an increase in CXCL1 protein within the blood serum (**F**) at day 7 p.i. as measured by ELISA. (**G**) Immunofluorscence analysis (original magnification ×40) of spinal cord tissue from Dox-treated double-tg mice confirmed that astrocytes were the source of CXCL1 production at day 7 p.i. (**H**) No significant changes in proinflammatory gene expression between double-tg and single-tg mice were observed within the spinal cord at day 12 p.i. using an RNA superarray. Data from (B) represent two experiments with a minimum of four mice per group. All quantitative real-time PCR samples were run in triplicate. (D) and (E) represent a minimum of three mice per group. Superarray data were compiled used the average value of two mice per group run in duplicate. Data are presented as average ± SEM; statistical significance was measured using an unpaired two-tailed Student *t* test. $*p < 0.05$, $**p < 0.01$.

not exert a direct antiviral effect on infected glial cells (data not shown). Collectively, these data indicate that the augmented clinical disease severity in Dox-treated double-tg mice is not a result of an inability to control viral replication within the CNS.

Neutrophil migration to the CNS is increased in Dox-treated double-tg mice

We have previously shown that neutrophils migrate into the CNS of JHMV-infected mice through a CXCR2-dependent mechanism (4). Therefore, we determined whether Dox-induced CXCL1 overexpression within the CNS resulted in enhanced mobilization of neutrophils to the CNS in response to JHMV infection. JHMV-infected double-tg and single-tg mice were i.c. infected with virus, treated with Dox, and mice were sacrificed at days 4 and 7 p.i. and neutrophil ($Ly6G^{hi}CD11b^{+}$) levels in blood were measured by flow cytometry. CXCL1 overexpression from the CNS resulted in significantly increased frequency of neutrophils within the blood at days 4 ($p < 0.05$) and 7 ($p < 0.001$) p.i. in double-tg mice compared with infected single-tg controls (Fig. 4A). Dox-induced CXCL1 production in JHMV-infected

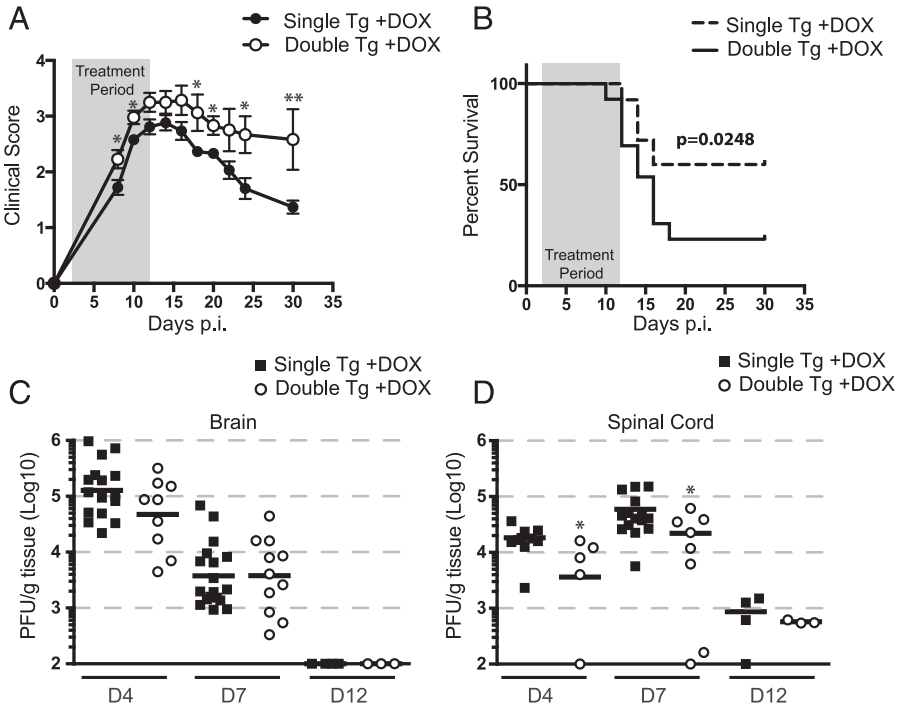

FIGURE 3. CXCL1 overproduction amplifies JHMV-induced clinical disease and mortality but is not a result of delayed viral clearance. Double-tg and single-tg mice were infected with 250 PFU JHMV and treated with 50 mg/kg Dox daily starting at day 2 p.i. through day 12 p.i. (**A**) Clinical severity was assessed until day 30 p.i. using a four-point scale. (**B**) Dox treatment of double-tg mice led to significantly increased mortality compared with Dox-treated single-tg controls. Viral titers of Dox-treated double-tg and single-tg mice were measured within both the brain (**C**) and spinal cord (**D**) by plaque assay. Each symbol represents one individual mouse; solid black lines represent geometric means. Statistical significance was measured with the Mann–Whitney *U* test. Clinical disease and mortality scoring represents an average of double-tg and single-tg mice. For (A) and (B), $n = 23$ single-tg mice and $n = 12$ double-tg mice. Statistical significance for the clinical scoring data was determined by a Student *t* test for each time point assessed. Statistical comparison of the survival curves was measured using the Mantel–Cox test. $*p < 0.05$, $**p < 0.01$.

double-tg mice also resulted in a significant increase in neutrophil frequency within the brain at days 4 ($p < 0.0001$) and 7 ($p < 0.01$) p.i. (Fig. 4B). Similarly, there was an increase in neutrophil frequency within spinal cords of double-tg mice at days 4 ($p < 0.01$) and 7 ($p < 0.05$) p.i. compared with single-tg mice (Fig. 4C). Immunofluorescence staining for neutrophils (Ly6B.2) supported the flow cytometric data and revealed increased numbers of neutrophils accumulating within the meninges of double-tg mice at day 7 p.i. (Fig. 4D). The increased presence of neutrophils within the CNS of double-tg mice suggested that there would also be a corresponding increase in BBB permeability. Rather, no differences were observed in BBB permeability within the brain or spinal cord at day 4 p.i. as measured by NaFl uptake (Fig. 4E) and at day 7 p.i. (data not shown). We also determined whether Dox-induced expression of CXCL1 affected mobilization and migration of $Ly6C^+$ monocytes to the CNS, as previous studies revealed an important role for these cells in amplifying the severity of autoimmune-mediated demyelination (18). There were no significant differences in the frequency $CD11b^+Ly6C^+Ly6G^-$ cells within the blood or brains of Dox-treated double-tg mice as compared with single-tg mice at defined times after infection with JHMV as determined by flow cytometric analysis (Fig. 4F, 4G). However, there was a slight but significant ($p < 0.05$) decrease in numbers of $CD11b^+Ly6C^+Ly6G^-$ cells within the spinal cords of Dox-treated double-tg mice at day 12 p.i. compared with single-tg mice (Fig. 4G) There were no differences in numbers of $CD11b^+Ly6C^+Ly6G^-$ cells within the blood or CNS of Dox-treated double-tg mice compared with single-tg mice (data not shown).

Demyelination is increased in response to elevated CNS expression of CXCL1

Examination of spinal cords from JHMV-infected, Dox-treated double-tg mice revealed an overall increase ($p < 0.05$) in the severity of demyelination when compared with infected single-tg animals (Fig. 5A). Analysis of defined spinal cord sections revealed increased demyelination along the length of the spinal cords of infected double-tg mice compared with single-tg mice, although pathology was enhanced within the upper thoracic region and to a lesser extent within the lower thoracic/lumbar regions (Fig. 5A). The increase in demyelination in double-tg mice was associated with a significant ($p < 0.05$) loss of mature oligodendrocytes (as determined by expression of GST-π) within the spinal cords (Fig. 5B). Additionally, there were increased numbers of microglia ($CD45^{lo}F4/80^+$) cells in Dox-treated, JHMV-infected double-tg mice compared with infected single-tg mice within the spinal cord as determined by flow cytometry as well as immunohistochemical staining for Iba1 (Fig. 5C). Immunophenotyping cells infiltrating into the brain via flow cytometry revealed no differences in the frequencies or numbers of $CD45^{hi}$ cells at defined times after infection (Supplemental Fig. 1). Within the spinal cord, there was a significant increase in the frequency of $CD45^{hi}$ infiltrates at day 4 p.i. and reflects the early enhancement of neutrophils in double-tg mice treated with Dox (Supplemental Fig. 1). However, there were no differences in $CD4^+$ T cells (Supplemental Fig. 1), $CD8^+$ T cells (Supplemental Fig. 1), or virus-specific $CD4^+$ (Supplemental Fig. 1) or $CD8^+$ T cells (Supplemental Fig. 1) infiltration into the brain or spinal cords of experimental mice. Overexpression of CXCL1 in Dox-treated, JHMV-infected double-tg mice did not increase numbers of infiltrating macrophages

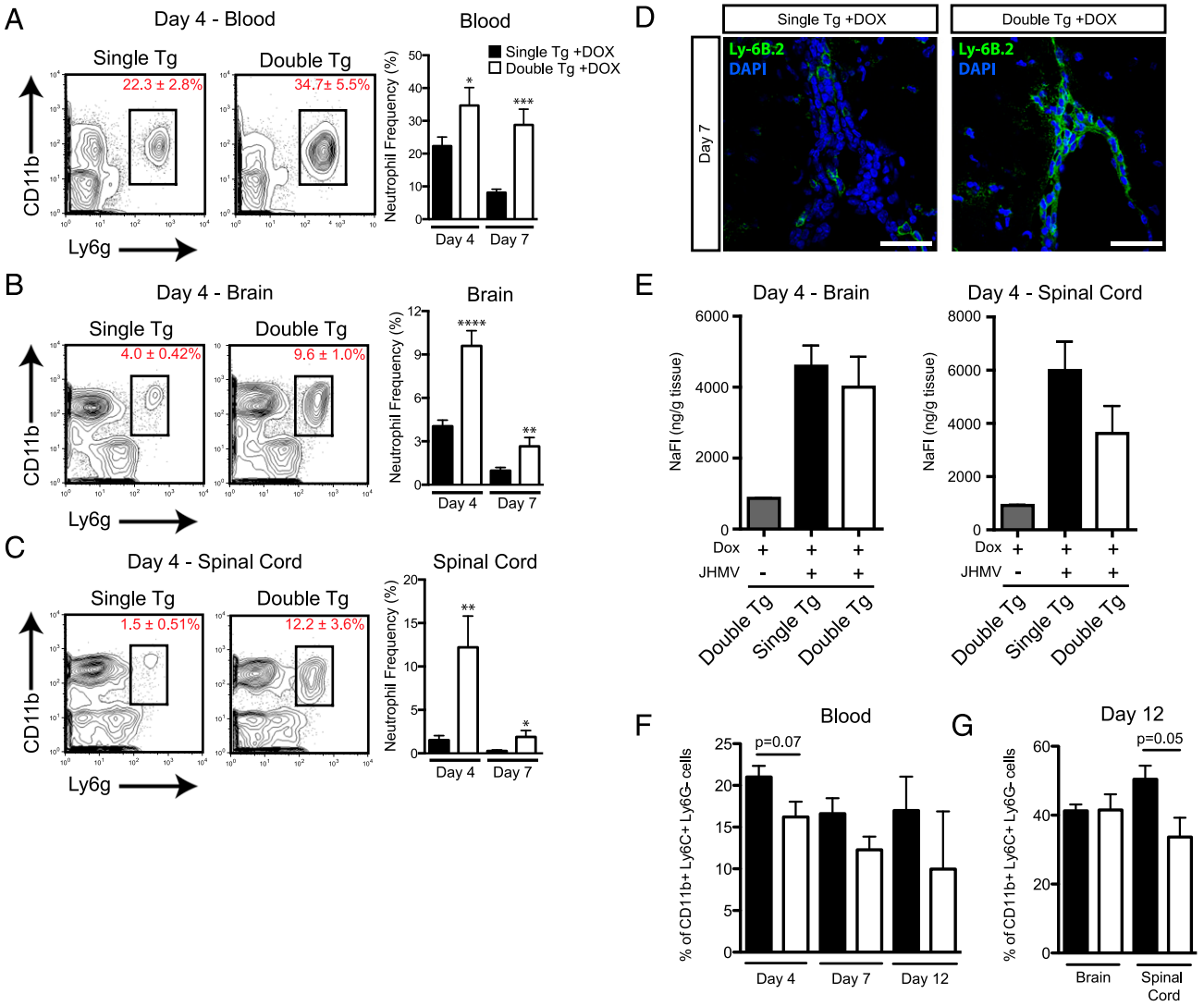

FIGURE 4. CXCL1 overproduction from astrocytes mobilizes neutrophils and directs them to the CNS. Blood from Dox-treated, JHMV-infected double-tg and single-tg mice was isolated at day 4 and day 7 p.i. and used for flow cytometric analysis. (**A**) The frequency of $CD11b^{+}Ly6G^{+}$ neutrophils was significantly higher within the blood at days 4 and 7 p.i. Neutrophil migration to the brains (**B**) and spinal cords (**C**) of both groups was assessed by flow cytometry at days 4 and 7 p.i. A significant increase in neutrophil frequency within the brain and spinal cord was observed in Dox-treated double-tg mice at both time points. (**D**) Immunofluorescence analysis indicated that $Ly6B.2^{+}$ neutrophils were primarily located at the ependymal lining and perivascular space at the spinal cord, with minimal neutrophil presence within the parenchyma. Scale bars, 50 μM. (**E**) At day 4 p.i., brains and spinal cords from Dox-treated single-tg and double-tg mice treated with NaFl were removed and total NaFl uptake was measured. No differences in the frequency of $CD11b^{+}Ly6C^{+}Ly6G^{-}$ cells were detected within either the blood (**F**) or brain and spinal cords (**G**) between Dox-treated double-tg or single-tg mice at defined times after infection with JHMV. (A)–(C) represent three independent experiments with a minimum of three mice per group per experiment at each time point analyzed; (F) and (G) represent two independent experiments with a minimum of three mice per group per experiment at each time point analyzed. Data are presented as average ± SEM; statistical significance was measured using an unpaired two-tailed Student *t* test. $*p < 0.05$, $**p < 0.01$, $***p < 0.001$, $****p < 0.0001$.

($CD45^{hi}F4/80^{+}$) in either the brains (Supplemental Fig. 2) or spinal cords (Supplemental Fig. 2) as compared with infected single-tg mice (Supplemental Fig. 2). Additionally, no differences were detected in expression of activation markers MHC class II (Supplemental Fig. 2) or CD80 (Supplemental Fig. 2), arguing that overexpression of CXCL1 in response to Dox treatment was not enhancing the activation state of inflammatory macrophages that contributed to increased myelin destruction.

Neutrophil accumulation within the spinal cord correlates with increased demyelination

We next determined whether neutrophil infiltration into the CNS was associated with the increase in both clinical and histologic disease in double-tg mice. Flow cytometric data indicated that neutrophil frequencies within the spinal cords of infected double-tg mice were significantly increased ($p < 0.01$) as well as their total numbers ($p < 0.001$) at day 12 p.i. compared with single-tg mice (Fig. 6A). CXCL1 expression, as determined by immunohistochemical staining, was elevated within the spinal cords of Dox-treated double-tg mice as compared with treated single-tg mice (Fig. 6B). Correspondingly, in double-tg mice, a significant increase in neutrophils ($p < 0.05$) was detected within the spinal cord parenchyma of double-tg mice compared with single-tg mice (Fig. 6C, 6D). Notably, neutrophils were enriched within the upper thoracic region of the spinal cord undergoing demyelination whereas these cells were relatively absent in demyelinating lesions in single-tg mice (Fig. 6E). To determine whether the robust parenchymal presence of neutrophils within the spinal cords of double-

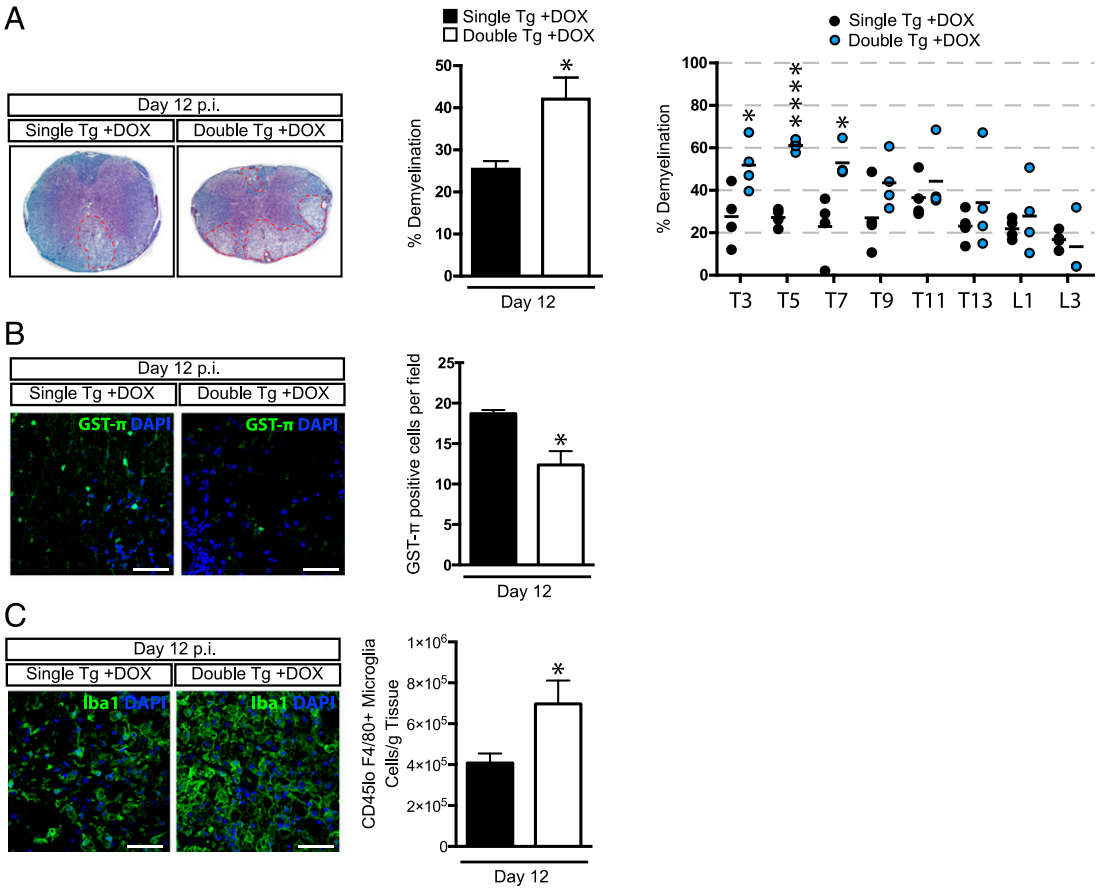

FIGURE 5. Elevated CXCL1 expression is associated with increased demyelination. Histopathological analysis of spinal cords of double-tg mice reveals an increase in demyelination. (**A**) Representative Luxol fast blue–stained spinal cords (original magnification ×4) reveal increased ($p < 0.05$) demyelination in Dox-treated double-tg mice compared with single-tg controls. Assessment of demyelination in defined spinal cord sections indicates white matter damage is more concentrated within the upper thoracic (T) regions (T3–T7) compared with lower T9–T13 as well as lumbar (L) regions examined. (**B**) Increased demyelination was associated with a reduction in the number total GST-π^+ oligodendrocytes within the white matter. The dot plot presented in (A) represents the percentage demyelination at specific anatomical regions of the spinal cord. (**C**) Immunofluorescence staining for Iba1 revealed increased numbers of positive cells within areas of demyelination in spinal cords of double-tg compared with single-tg mice at day 12 p.i., and flow analysis indicated increased ($p < 0.05$) numbers of microglia ($CD45^{lo}F4/80^+$). Scale bars, 50 μM. (A)–(C) represent a minimum of four mice per group. Data are presented as average ± SEM; statistical significance was measured using an unpaired two-tailed Student *t* test. $*p < 0.05$.

tg mice was associated with the enhanced lesion load, neutrophils were eliminated from the periphery using anti-Ly6g mAb injection from days 3 to 15 p.i. (Fig. 7A). Flow analysis of immune cell infiltrates within the spinal cord confirmed neutrophil depletion following anti-Ly6g treatment (Fig. 7A). Supporting our previous findings that double-tg mice display an increase in white matter demyelination compared with single-tg mice was the observation that isotype-treated double-tg mice displayed a significant increase ($p < 0.001$) in the percentage of total white matter demyelination compared with anti-Ly6g–treated single-tg mice (Fig. 7B).

Discussion

The ELR^+ CXC chemokines (CXCL1–3 and CXCL5–8) are high-affinity ligands for their cognate receptor CXCR2. This signaling axis serves critical functions in host defense and disease, as it is the dominant chemotactic pathway for neutrophil homing to sites of inflammation. CXCL1, CXCL2, and CXCL5 are upregulated within the CNS shortly following JHMV infection and control neutrophil migration to the BBB, resulting in peak accumulation by 3 d p.i (4). The importance of neutrophils in host defense to JHMV infection has been investigated with the use of Abs that either eliminate neutrophils from the periphery or prevent their chemotaxis to the CNS. Many of these studies (4, 19, 20) have implicated the short-lived neutrophils as a primarily cellular source for the protease MMP9 during acute JHMV infection. However, no studies have investigated how chronic ELR chemokine overproduction from the CNS impacts neutrophil function as well as host defense and disease following JHMV infection.

The successful generation of a Dox-dependent CXCL1-expressing tg mouse has allowed for selective CXCL1 production from astrocytes within mice infected with JHMV. Dox administration resulted in elevated CXCL1 transgene expression within the brains and spinal cords of double-tg mice, correlating with rapid and selective neutrophil migration to the CNS compared with Dox-treated controls. As a result of CXCL1 transgene expression, double-tg mice displayed a sustained increase in clinical disease severity congruent with an increase in mortality. This observation shares similarities to mice infected with the lethal DM-JHMV variant that is characterized by a severe disease whereby neutrophils dominate the immune cell composition early following infection (20). Overaccumulation of neutrophils in the CNS did not result in an increase in BBB permeability or affect the expression of proinflammatory factors that could potentially attract inflammatory leukocytes. Indeed, we observed

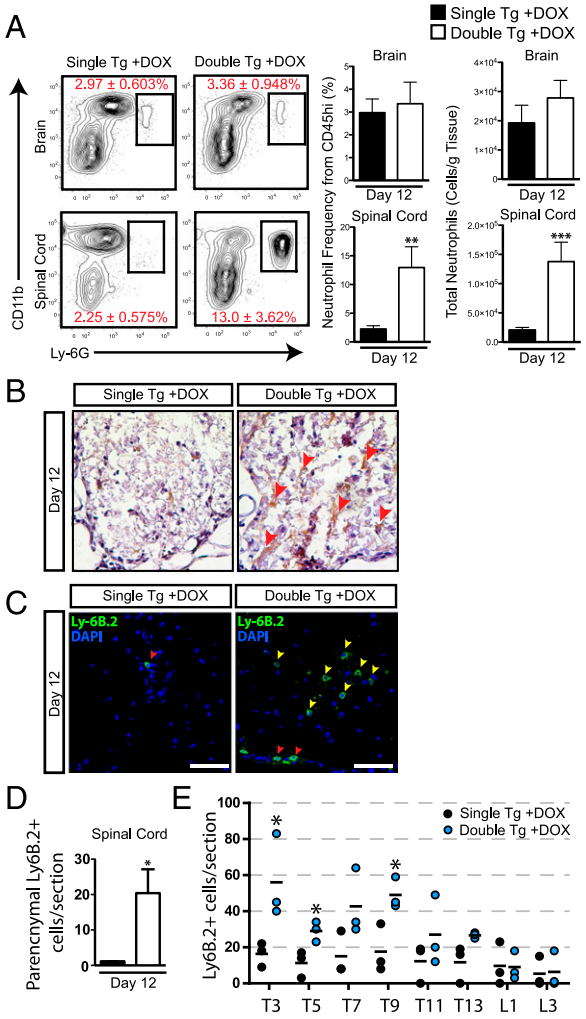

FIGURE 6. Neutrophils are found within parenchymal regions of the spinal cord in double-tg mice. (**A**) At day 12 p.i. brains and spinal cords were isolated and single-cell suspensions were prepared from double-tg and single-tg mice infected with JHMV. Flow cytometric analysis revealed a significant increase in the frequency and total number of neutrophils within the spinal cord of double-tg mice. (**B**) CXCL1 protein was detected by immunohistochemical staining (red arrowheads) within spinal cords of Dox-treated double-tg mice, and (**C**) immunofluorescence staining further demonstrated a significant increase in the number of Ly6B.2$^+$ neutrophils (yellow arrowheads). Scale bars, 50 μM. (**D**) Quantification of neutrophils within the spinal cords indicated an overall increase ($p < 0.05$) in Dox-treated double-tg mice compared with Dox-treated single-tg mice. (**E**) Quantification of neutrophils in defined anatomic regions of spinal cords showed increased numbers of neutrophils ($p < 0.05$) within upper thoracic (T) regions (T3–T9) and lower numbers at T11–T13 and lumbar (L) regions in Dox-treated double-tg mice compared with Dox-treated single-tg mice. (A) represents three independent experiments with a minimum of three mice per group per experiment. (D) and (E) represent a minimum of three mice per group. Data are presented as average ± SEM; statistical significance was measured using an unpaired two-tailed Student *t* test. *$p < 0.05$.

no statistical difference in the frequencies of macrophages or T cells between double-tg and single-tg mice at day 12 p.i. as measured by flow cytometry. These results are partially supported by Savarin et al. (7, 8) who have provided evidence that neutrophils are not essential for promoting access of activated immune cells into the CNS, as neutropenic mice or MMP9-deficient mice infected with sublethal strains of JHMV do not show appreciable differences in the early recruitment of activated leukocytes into the parenchyma. Overall, these data indicate that the increased presence of neutrophils within the CNS following JHMV infection does not influence BBB integrity and has no impact on the recruitment of other inflammatory cells from the periphery. Importantly, Dox-induced CXCL1 within the CNS did not affect mobilization of CD11b$^+$Ly6C$^+$Ly6G$^-$ monocytes within the blood or migration into the CNS. Rather, there were decreased numbers of these cells within the spinal cords of Dox-treated double-tg mice compared with single-tg mice by day 12 p.i. Whether CXCL1 modulates trafficking of CD11b$^+$Ly6C$^+$Ly6G$^-$ monocytes in chronic stages of CNS inflammatory disease is not known at this time.

An increase in the severity of white matter demyelination was observed at day 12 p.i. in Dox-treated double-tg mice, and this correlated with an overall decrease in the total number of GST-π$^+$ mature oligodendrocytes. We do not think that CXCL1 had any direct cytotoxic activity on oligodendroglia, as we have previously

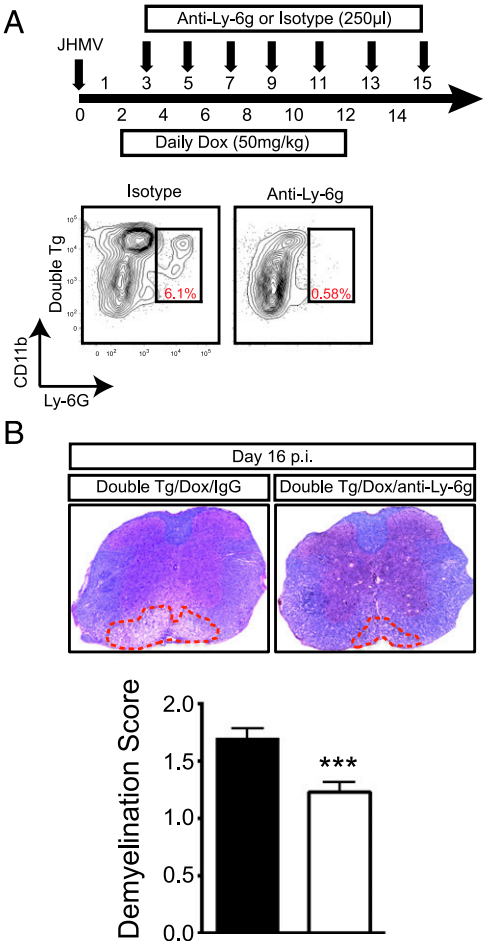

FIGURE 7. Neutrophils amplify the severity of demyelination. (**A**) Dox-treated JHMV-infected double-tg mice were treated with either anti-Ly6g Ab or isotype-matched control starting between days 3 and 4 p.i. and continuing every other day until day 15 p.i. Representative flow analysis of spinal cords confirmed anti-Ly6G treatment successfully depleted neutrophils. (**B**) Representative Luxol fast blue–stained spinal cord sections from JHMV-infected double-tg mice treated with either control IgG2a or anti-Ly6G Ab between days 3 and 15 p.i. Quantification of the severity of demyelination revealed reduced white matter damage in mice treated with anti-Ly6G Ab compared with mice treated with isogenic IgG2a control Ab; data are derived from two independent experiments with a minimum of three mice per group per experiment. Data are presented as average ± SEM; statistical significance was measured using an unpaired two-tailed Student *t* test. *$p < 0.001$.

shown that treatment of differentiating mouse oligodendrocyte progenitor cells with recombinant CXCL1 does not kill these cells (21). However, our findings revealed a significant parenchymal presence of neutrophils associated with regions of severe demyelination in JHMV-infected double-tg mice, and ablation of these cells limited the severity of white matter damage, arguing for an important role for neutrophils in amplifying disease. Although recent studies suggest that Ly6C$^+$ myeloid precursor cells play a pathogenic role during autoimmune demyelination (17), our findings reveal that the increase in tissue damage was not the result of enhanced migration of these cells to the CNS of Dox-treated double-tg mice when compared with single-tg mice. Neutrophils are known to possess an arsenal of proteases and toxic factors that can impact cell survival, including neutrophil elastase, cathepsin G, and MMPs (22). Moreover, respiratory burst from the neutrophil phagosome and the generation NO as well as reactive oxygen species through the NADPH oxidase complex can contribute to both vascular and parenchymal damage, resulting in bystander destruction of axons and oligodendrocytes within white matter tissue (23, 24). This has been demonstrated in mouse models of ischemic injury where inhibition of the NADPH complex results in less injury to vascular endothelium and reduced cellular damage within brain parenchyma (25). Furthermore, neutrophils are implicated in exacerbating lesion development within spinal cords on patients with neuromyelitis optica (26), and inhibition of neutrophil elastase, a serine protease released from the primary granules of neutrophils, within mouse models of neuromyelitis optica resulted in reduced neuroinflammation and myelin loss (27, 28). The potential destructive force of neutrophils has also been demonstrated using neurovirulent JHM recombinant variants, as neutrophil depletion or inhibition of NO synthase correlated with reduced apoptosis of glial cells within the brain (29). Another scenario is that neutrophils could be promoting pathology by drawing in macrophages within more cervical and upper thoracic regions of the spinal cord. Within the EAE model of chronic neurologic disease, neutrophils have recently been reported to have a role in maturating local APCs within the CNS, thus potentially contributing to enhanced disease severity by increasing numbers of autoreactive T cells (30). We observed dense clusters of macrophages in heavily demyelinated white matter regions that also contained significant neutrophil populations in double-tg mice. However, we think it unlikely that the increase in disease severity is the result of macrophages presenting viral Ag, as we did not detect elevated numbers of virus-specific T cells within either the brain or spinal cord.

Tani et al. (31) have shown that chronic overexpression of CXCL1 from oligodendrocytes within naive mice results in a neurologic disease associated with microglia and astrocytic reactivity as a result of pronounced neutrophil accumulation within the brain. Indeed, we observed increased numbers of microglia within infected double-tg mice, and astrocytes displayed distinct phenotypic changes within heavily demyelinated regions, including truncated morphologies and hypertrophy (unpublished observations). We are currently evaluating how microglia may augment demyelination and whether this is dependent on the presence of neutrophils. More importantly, these findings argue that sustained neutrophil infiltration into the CNS enhances clinical disease severity associated with an increase in white matter destruction. Additionally, our observations are consistent with recent studies from Segal and colleagues (32) and argue that therapies targeting neutrophil accumulation within the CNS may offer novel alternative therapies for treating neuroinflammatory diseases.

Acknowledgments

We thank Colleen Worne for outstanding technical assistance.

Disclosures

The authors have no conflicts of interest.

References

1. Bergmann, C. C., T. E. Lane, and S. A. Stohlman. 2006. Coronavirus infection of the central nervous system: host-virus stand-off. *Nat. Rev. Microbiol.* 4: 121–132.
2. Liu, M. T., B. P. Chen, P. Oertel, M. J. Buchmeier, D. Armstrong, T. A. Hamilton, and T. E. Lane. 2000. The T cell chemoattractant IFN-inducible protein 10 is essential in host defense against viral-induced neurologic disease. *J. Immunol.* 165: 2327–2330.
3. Lane, T. E., M. T. Liu, B. P. Chen, V. C. Asensio, R. M. Samawi, A. D. Paoletti, I. L. Campbell, S. L. Kunkel, H. S. Fox, and M. J. Buchmeier. 2000. A central role for CD4$^+$ T cells and RANTES in virus-induced central nervous system inflammation and demyelination. *J. Virol.* 74: 1415–1424.
4. Hosking, M. P., L. Liu, R. M. Ransohoff, and T. E. Lane. 2009. A protective role for ELR$^+$ chemokines during acute viral encephalomyelitis. *PLoS Pathog.* 5: e1000648.
5. Lane, T. E., V. C. Asensio, N. Yu, A. D. Paoletti, I. L. Campbell, and M. J. Buchmeier. 1998. Dynamic regulation of α- and β-chemokine expression in the central nervous system during mouse hepatitis virus-induced demyelinating disease. *J. Immunol.* 160: 970–978.
6. Hosking, M. P., E. Tirotta, R. M. Ransohoff, and T. E. Lane. 2010. CXCR2 signaling protects oligodendrocytes and restricts demyelination in a mouse model of viral-induced demyelination. *PLoS One* 5: e11340.
7. Savarin, C., S. A. Stohlman, R. Atkinson, R. M. Ransohoff, and C. C. Bergmann. 2010. Monocytes regulate T cell migration through the glia limitans during acute viral encephalitis. *J. Virol.* 84: 4878–4888.
8. Savarin, C., S. A. Stohlman, A. M. Rietsch, N. Butchi, R. M. Ransohoff, and C. C. Bergmann. 2011. MMP9 deficiency does not decrease blood-brain barrier disruption, but increases astrocyte MMP3 expression during viral encephalomyelitis. *Glia* 59: 1770–1781.
9. Yu, J., L. Zhang, P. M. Hwang, C. Rago, K. W. Kinzler, and B. Vogelstein. 1999. Identification and classification of p53-regulated genes. *Proc. Natl. Acad. Sci. USA* 96: 14517–14522.
10. Hirano, N., T. Murakami, K. Fujiwara, and M. Matsumoto. 1978. Utility of mouse cell line DBT for propagation and assay of mouse hepatitis virus. *Jpn. J. Exp. Med.* 48: 71–75.
11. Schwartz, J. P., and D. J. Wilson. 1992. Preparation and characterization of type 1 astrocytes cultured from adult rat cortex, cerebellum, and striatum. *Glia* 5: 75–80.
12. Tirotta, E., P. Duncker, J. Oak, S. Klaus, M. R. Tsukamoto, L. Gov, and T. E. Lane. 2013. Epstein-Barr virus-induced gene 3 negatively regulates neuroinflammation and T cell activation following coronavirus-induced encephalomyelitis. *J. Neuroimmunol.* 254: 110–116.
13. Blanc, C. A., H. Rosen, and T. E. Lane. 2014. FTY720 (fingolimod) modulates the severity of viral-induced encephalomyelitis and demyelination. *J. Neuroinflammation* 11: 138.
14. Chen, L., R. Coleman, R. Leang, H. Tran, A. Kopf, C. M. Walsh, I. Sears-Kraxberger, O. Steward, W. B. Macklin, J. F. Loring, and T. E. Lane. 2014. Human neural precursor cells promote neurologic recovery in a viral model of multiple sclerosis. *Stem Cell Rep.* 2: 825–837.
15. Kang, Z., C. Wang, J. Zepp, L. Wu, K. Sun, J. Zhao, U. Chandrasekharan, P. E. DiCorleto, B. D. Trapp, R. M. Ransohoff, and X. Li. 2013. Act1 mediates IL-17-induced EAE pathogenesis selectively in NG2$^+$ glial cells. *Nat. Neurosci.* 16: 1401–1408.
16. Glabinski, A. R., M. Krakowski, Y. Han, T. Owens, and R. M. Ransohoff. 1999. Chemokine expression in GKO mice (lacking interferon-γ) with experimental autoimmune encephalomyelitis. *J. Neurovirol.* 5: 95–101.
17. Glabinski, A. R., V. K. Tuohy, and R. M. Ransohoff. 1998. Expression of chemokines RANTES, MIP-1α and GRO-α correlates with inflammation in acute experimental autoimmune encephalomyelitis. *Neuroimmunomodulation* 5: 166–171.
18. King, I. L., T. L. Dickendesher, and B. M. Segal. 2009. Circulating Ly-6C$^+$ myeloid precursors migrate to the CNS and play a pathogenic role during autoimmune demyelinating disease. *Blood* 113: 3190–3197.
19. Zhou, J., N. W. Marten, C. C. Bergmann, W. B. Macklin, D. R. Hinton, and S. A. Stohlman. 2005. Expression of matrix metalloproteinases and their tissue inhibitor during viral encephalitis. *J. Virol.* 79: 4764–4773.
20. Zhou, J., S. A. Stohlman, D. R. Hinton, and N. W. Marten. 2003. Neutrophils promote mononuclear cell infiltration during viral-induced encephalitis. *J. Immunol.* 170: 3331–3336.
21. Tirotta, E., R. M. Ransohoff, and T. E. Lane. 2011. CXCR2 signaling protects oligodendrocyte progenitor cells from IFN-γ/CXCL10-mediated apoptosis. *Glia* 59: 1518–1528.
22. Mantovani, A., M. A. Cassatella, C. Costantini, and S. Jaillon. 2011. Neutrophils in the activation and regulation of innate and adaptive immunity. *Nat. Rev. Immunol.* 11: 519–531.
23. Hampton, M. B., A. J. Kettle, and C. C. Winterbourn. 1998. Inside the neutrophil phagosome: oxidants, myeloperoxidase, and bacterial killing. *Blood* 92: 3007–3017.

24. Weiss, S. J. 1989. Tissue destruction by neutrophils. *N. Engl. J. Med.* 320: 365–376.
25. Chen, H., Y. S. Song, and P. H. Chan. 2009. Inhibition of NADPH oxidase is neuroprotective after ischemia-reperfusion. *J. Cereb. Blood Flow Metab.* 29: 1262–1272.
26. Lucchinetti, C. F., R. N. Mandler, D. McGavern, W. Bruck, G. Gleich, R. M. Ransohoff, C. Trebst, B. Weinshenker, D. Wingerchuk, J. E. Parisi, and H. Lassmann. 2002. A role for humoral mechanisms in the pathogenesis of Devic's neuromyelitis optica. *Brain* 125: 1450–1461.
27. Zhang, H., J. L. Bennett, and A. S. Verkman. 2011. Ex vivo spinal cord slice model of neuromyelitis optica reveals novel immunopathogenic mechanisms. *Ann. Neurol.* 70: 943–954.
28. Saadoun, S., P. Waters, C. MacDonald, B. A. Bell, A. Vincent, A. S. Verkman, and M. C. Papadopoulos. 2012. Neutrophil protease inhibition reduces neuromyelitis optica-immunoglobulin G-induced damage in mouse brain. *Ann. Neurol.* 71: 323–333.
29. Iacono, K. T., L. Kazi, and S. R. Weiss. 2006. Both spike and background genes contribute to murine coronavirus neurovirulence. *J. Virol.* 80: 6834–6843.
30. Steinbach, K., M. Piedavent, S. Bauer, J. T. Neumann, and M. A. Friese. 2013. Neutrophils amplify autoimmune central nervous system infiltrates by maturing local APCs. *J. Immunol.* 191: 4531–4539.
31. Tani, M., M. E. Fuentes, J. W. Peterson, B. D. Trapp, S. K. Durham, J. K. Loy, R. Bravo, R. M. Ransohoff, and S. A. Lira. 1996. Neutrophil infiltration, glial reaction, and neurological disease in transgenic mice expressing the chemokine N51/KC in oligodendrocytes. *J. Clin. Invest.* 98: 529–539.
32. Rumble, J. M., A. K. Huber, G. Krishnamoorthy, A. Srinivasan, D. A. Giles, X. Zhang, L. Wang, and B. M. Segal. 2015. Neutrophil-related factors as biomarkers in EAE and MS. *J. Exp. Med.* 212: 23–35.